Final Draft
of the original manuscript:

Huang, Z.; Wang, L.; Zhou, B.; Fischer, T.; Yi, S.; Zeng, X.:
Observation of non-basal slip in Mg-Y by in situ three-dimensional X-ray diffraction
In: Scripta Materialia (2017) Elsevier

DOI: 10.1016/j.scriptamat.2017.09.011

Observation of non-basal slip in Mg-Y by in situ three-dimensional X-ray diffraction

Zhonghe Huang[a], Leyun Wang[a,b,*], Bijin Zhou[a], Torben Fischer[b], Sangbong Yi[c], Xiaoqin Zeng[d,*]

[a] *School of Materials Science and Engineering, Shanghai Jiao Tong University, Shanghai, 200240 China*

[b] *Institute of Materials Research, Helmholtz-Zentrum Geesthacht, 21502 Geesthacht, Germany*

[c] *Magnesium Innovation Centre, Helmholtz-Zentrum Geesthacht, 21502 Geesthacht, Germany*

[d] *The State Key Laboratory of Metal Matrix Composites, Shanghai Jiao Tong University, Shanghai, 200240 China*

* Corresponding author

leyunwang@sjtu.edu.cn and xqzeng@sjtu.edu.cn

Abstract

Mg-5wt%Y extruded alloy showed excellent tensile ductility along the extrusion direction. An in situ tensile test with three-dimensional X-ray diffraction (3DXRD) identified prismatic, basal, and pyramidal <a> slip in different grains during deformation based on the analysis of grain rotation. Ex situ slip trace analysis using electron backscatter diffraction confirms the extensive activation of non-basal slip systems, which can explain the high ductility of this material. Critical resolved shear stress (CRSS) ratios between non-basal slip and basal slip are estimated from Schmid factor analysis.

Keywords

Magnesium alloys; synchrotron radiation; 3DXRD; plastic deformation; slip

Text

As the lightest structural metallic material, Mg alloys have gained growing attention in the automobile industry for fuel efficiency [1]. However, room temperature ductility of Mg alloys still needs improvement to reduce the production cost [2]. Recent studies have shown that the addition of rare earth (RE) elements can improve the ductility of Mg alloys by weakening the basal-type texture [3-5] and reducing the critical resolved shear stress (CRSS) of non-basal slip in relative to basal slip [6-8]. Sandlöbes et al. [9] identified a high activity of pyramidal <c+a> dislocations in a Mg-3wt%Y alloy by transmission electron microscopy (TEM), which was attributed to the reduction of the stacking fault energy (SFE) by Y and those stacking faults serving as nucleation sites for <c+a> dislocations [10,11]. This mechanism for <c+a> dislocation nucleation was further explored by Agnew et al. [12] using continuum elasticity-based dislocation theory. In a molecular dynamics (MD) study, Kim et al. [13] found that Y impedes the movement of basal <a> dislocation more strongly than pyramidal <c+a> dislocation, which is an alternative explanation for the high activity of <c+a> dislocations in Mg-Y. Stanford et al. [6] quantitatively evaluated the effect of Y on CRSS for various slip modes in Mg using in situ neutron diffraction. Their result, however, suggested that the CRSS of pyramidal <c+a> slip is still 10 times higher than that of basal slip in a Mg-2.2wt%Y, which implies that <c+a> slip may have a limited role in explaining the high ductility of Mg-Y alloys. In a recent first-principles study, Tsuru and Chrzan [14] found that Y can stabilize the screw <a> dislocation compact core in Mg and thus enable cross-slip of <a> dislocations from the basal plane to non-basal planes. This mechanism has not been experimentally investigated so far.

Three-dimensional X-ray diffraction (3DXRD) is a novel technique to analyze the meso-scale deformation of polycrystalline materials. Compared with electron microscopy, 3DXRD allows a non-destructive and dynamic characterization of grain structure and grain-by-grain stress state in the bulk material [15]. In situ 3DXRD has been used to study grain-level stress heterogeneity [16], twin nucleation [17-20], and in-grain orientation gradient [21, 22] in metals under deformation.

In the present paper, slip activity in individual grains in a Mg-Y alloy is studied by in situ 3DXRD. Both basal slip and non-basal <a> slip are identified in different grains based on the analysis of grain rotation. The CRSS ratio between non-basal <a> slip and basal slip is further estimated from Schmid factor (SF) analysis.

A binary Mg-5wt%Y alloy was produced by casting. The billets were solution treated at 540°C for 24 h, extruded at 500°C (extrusion ratio = 18:1), and finally annealed at 530°C for 25 min. The average grain size in the final state was approximately 100μm. Tensile specimens with the gauge dimension of 4mm×1mm×1mm (L×W×T) were fabricated from the extruded rod, with the tensile axis being parallel to the extrusion direction (ED). The in situ 3DXRD experiment was performed at the P07 beamline of PETRA III at the Deutsches Elektronen-Synchrotron (DESY) facility. Figure 1 shows a schematic of the experimental setup. A monochromatic X-ray beam (width = 1.5mm, height = 100μm) with an energy of 45 keV was used to illuminate the specimen. To employ the 3DXRD technique, at each load step the specimen was rotated from -70.5° to +70.5° around the loading axis (Z) together with the pin-load tensile frame. At every 1° rotation interval, a diffraction pattern was collected using an X-ray VHR

camera (Photonic Science Ltd.). The X-ray camera has an array of 4008×2672 pixels with an effective pixel size of 30μm×30μm. The sample-to-camera distance was approximately 211mm. The specimen was deformed by tension up to 3.3% engineering strain with a total of 24 load steps and then deformed to its failure with 6 additional load steps (strain to failure ~15%). The stress-strain curve is shown in Figure 1. At each of the first 24 load steps, 3DXRD measurement was performed in two sequential layers along the specimen gauge. A digital image correlation (DIC) camera was used to ensure that approximately the same position on the gauge was measured through all load steps. Due to the increased smearing of the diffraction peaks, grain indexing from the 3DXRD data became more difficult after 2.0% of strain. Nevertheless, analysis of the deformation behavior up to 2.0% of strain already brings insights for the high ductility of this alloy. For comparison, similarly extruded pure Mg typically has a strain to failure of less than 5% under tension along ED.

Diffraction patterns collected at each load step were used to index grains in the illuminated volume using the FABLE software [23, 24]. Overall, three analysis programs — *PeakSearch*, *Transformation*, *GrainSpotter* — were used sequentially. These programs identify peaks above a certain intensity threshold, assign to each a reciprocal lattice vector, and index grains based on these reciprocal lattice vectors, respectively. An independent Matlab code [18] was additionally used to obtain the center of mass (COM) position on the X-Y plane (2 unknowns) and elastic strain tensor (6 unknowns) of each indexed grain using the position of all its diffraction peaks through least squares fitting. Due to the relatively small area of the X-ray camera used for this experiment, the number of identified diffraction peaks per grain was ~35, which is lower than that in similar 3DXRD experiments (e.g. 70-80

diffraction peaks per grain in [20]). This introduced a relatively large fitting error for COM position and elastic strain tensor. The average error bar for COM position (ΔX, ΔY) is 60 μm, which is still smaller than the average grain size of 100 μm. The fitting errors for elastic strain components are more severe: $\Delta e_{XX} = 3.3\times10^{-3}$, $\Delta e_{YY} = 1.9\times10^{-3}$, $\Delta e_{ZZ} = 1.3\times10^{-3}$, making it difficult to obtain a reliable grain-averaged stress tensor. On the other hand, the grain orientation determined by FABLE is more accurate, as there are only 3 unknowns (instead of 8) that need to be fitted using the same number of peaks. The average mean internal angle (meanIA) of each indexed grain is ~0.6°. By tracking the orientation evolution for selected grains during loading, we can identify the active slip mode in each of them.

Approximately 180 grains were indexed among the two layers (~90 grains in each layer). Figure 2 shows the {0001} pole figures and the COM maps of all indexed grains in the two layers at zero strain. The specimen shows a typical extrusion texture, where the <0001> axis of most grains are perpendicular to the extrusion direction (Z). The COMs of all indexed grains are within a 1200μm×1200μm square area, which is consistent with the 1mm×1mm cross-section area of the specimen. Nine grains that were tracked in most subsequent load steps were analyzed in detail for the slip activity in each of them.

To identify the activated slip system in a grain, we analyze how the grain orientation rotated during deformation. The difference in grain orientation between the initial state and each subsequent load step is defined as the disorientation value at that load step. The angular difference of the <0001> direction between the initial state and each subsequent load step is defined as the c-axis misalignment at that load step.

Mathematically, the c-axis misalignment of a grain should be always lower or equal to its disorientation at any step. Disorientation and c-axis misalignment evolution with the macroscopic engineering strain (ε) in Grains 1, 2 and 5 are shown in Figure 3 (a-c) up to 1.9% strain. A hexagonal prism illustrates the crystal orientation of each grain when viewing along the Z direction.

For Grain 1, its c-axis misalignment was always very close to the disorientation, increasing from 0 (at ε=0) to ~1.7° (at ε=1.9%). This indicates that the orientation rotation of Grain 1 was achieved by tilting its c-axis without rotation around the c-axis. Crystal orientation of Grain 1 at the load step when plastic deformation just started (ε=0.16%) and the last load step when it can still be identified (ε=1.9%) were compared. The orientation difference and the rotation axis between these two orientation values are calculated and shown in Table 1. The rotation axis is close to the [0, 1, 0] direction, which can result from either basal slip $(0001)[\bar{2}110]$ or pyramidal II <c+a> slip $(\bar{2}112)[\bar{2}11\bar{3}]$. From Schmid factor analysis (Table 1), the basal slip system (SF=0.394) is more likely the activated slip system than the <c+a> slip (SF=0.099). Grains 6 and 7 show a similar way of rotation as Grain 1. From Schmid factor analysis, they were also most likely deformed by basal slip.

For Grain 2, its c-axis misalignment closely followed the disorientation up to ε=0.1%. Further strain, however, separated the two values: the c-axis misalignment stayed around 0.1°, while the disorientation increases rapidly and eventually to ~0.6° at ε=1.4%. This indicates that the orientation rotation of Grain 2 was achieved by rotation around its c-axis. Such a behavior can only result from prismatic slip

$\{10\bar{1}0\}<1\bar{2}10>$. From Schmid factor analysis (Table 1), the activated slip system in Grain 2 is most likely $(1\bar{1}00)[11\bar{2}0]$. Grain 3 shows similar prismatic slip activity.

For Grain 5, after the plastic deformation started, both its disorientation and c-axis misalignment increased, but the disorientation increased at a faster pace than the c-axis misalignment. Neither basal slip nor prismatic slip can account for this type of orientation rotation. It is found that the rotation axis of Grain 5 during plastic deformation was around the direction of [0.02, -0.42, -0.91]. Activation of pyramidal <a> slip $(0\bar{1}11)[2\bar{1}\bar{1}0]$ would theoretically cause a grain to rotate around an axis of [0, -0.47, -0.88]. The observed rotation axis in Grain 5 being very close to that theoretical value indicates that pyramidal <a> slip with SF=0.499 was the dominant slip mode in Grain 5. Grains 4, 8, and 9 show similar way of crystal rotation. For Grains 8 and 9, the pyramidal <a> slip that can be responsible for the rotation axis also has a high Schmid factor (highest among all six pyramidal <a> slip systems). For Grain 4, however, that pyramidal <a> slip has a low Schmid factor of 0.116. That slip system could still be activated by local stress concentration. Another possibility is that the crystal rotation in Grain 4 was achieved by concurrent activation of basal slip $(0\bar{1}11)[2\bar{1}\bar{1}0]$ (SF=0.195) and prismatic slip $(10\bar{1}0)[1\bar{2}10]$ (SF=0.429).

To further verify the non-basal slip activity in this Mg-5wt%Y alloy, a separate specimen of this material was ground and polished, and then deformed up to 4.5% tensile strain. EBSD-based slip trace analysis (e.g. [25]) was performed on the deformed sample by a FEI NOVA NanoSEM 230 scanning electron microscope

(SEM). The identified slip systems in a few grains are shown in Figure 3(d-g). Slip lines in Grains G2, G3, and G8 correspond to the slip trace of basal slip. Slip lines in Grain G1 (Euler angles = (266º, 133º, 68º)) correspond to the slip traces of prismatic slip $(\bar{1}100)[11\bar{2}0]$ (SF=0.49) and pyramidal <a> slip $(\bar{1}101)[11\bar{2}0]$ (SF=0.45). The wavy slip lines indicate the occurrence of cross slip between these two slip systems with the same Burgers vector. Slip lines in Grain G7 (Euler angles = (220º, 153º, 50º)) correspond to the slip traces of pyramidal <a> slip $(\bar{1}101)[11\bar{2}0]$ (SF=0.42) and basal slip $(0001)[11\bar{2}0]$ (SF=0.30). EBSD-based slip trace analysis confirms that basal, prismatic and pyramidal <a> slip can all be activated in this Mg-5wt%Y alloy, which is consistent with the in situ 3DXRD experiment.

In order to estimate the CRSS ratio between non-basal slip modes and the basal slip mode, SF of basal, prismatic, and pyramidal <a> slip in Grains 1, 6, 7, 2, 3, 5, 8, and 9from the 3DXRD measurements were compared in Figure 4(a). From the above analysis, Grains 1, 6, and 7 were dominated by basal slip. In these three grains, SFs for basal slipare generally higher than the other grains in which prismatic slip or pyramidal <a> slip was activated. The comparison indicates that the slip activity in a grain strongly depends on the Schmid factor ratio between non-basal slip and basal slip. The ratios of $SF_{pyramidal\ <a>}/SF_{basal}$ and SF_{prism}/SF_{basal} were further calculated for these grains and shown in Figure 4(b). According to crystal plasticity theory, a slip system will be activated when the resolved shear stress (RSS) exceeds its CRSS value. Assuming the local stress in each grain is similar as the global tension stress on the specimen, the RSS on a slip system would be proportional to the SF. In that case, the ratio of $CRSS_{prism}/CRSS_{basal}$ in the examined Mg-5wt%Y alloy is estimated between

1.8 and 2.7 — had the ratio been less than 1.6, prismatic slip instead of basal slip would have been activated in Grain 6 whose SF_{prism}/SF_{basal} is approximately 1.8; had the ratio been greater than 2.7, basal slip rather than prismatic slip would have been developed in Grain 2 whose SF_{prism}/SF_{basal} is approximately 2.7. In a similar way, the ratio of $CRSS_{pyramidal\ <a>}/CRSS_{basal}$ is estimated between 1.6 and 1.8. The estimated ratios of $CRSS_{prism}/CRSS_{basal}$ and $CRSS_{pyramidal\ <a>}/CRSS_{basal}$ in this Mg-5wt%Y alloy are significantly lower than that in most Mg alloys (>10) [6, 26]. The reduced CRSS ratio between non-basal slip and basal slip can explain the excellent ductility of this alloy. Wavy slip lines are frequently observed in the deformed microstructure (e.g. Grain G1 and Grain G7 in Figure 3(d, f)), suggesting that cross-slip is relatively easy in this material. According to a recent study using density function theory (DFT) [14], Y is able to dramatically reduce the energy barrier for <a> dislocations to cross slip from the basal plane to non-basal planes. Detailed calculation in [14] estimated the ratio of $CRSS_{prism}/CRSS_{basal}$ to be ~1.5 in Mg-1.0at%Y (equivalent to Mg-3.6wt%Y). Our 3DXRD experiment result supports that prediction.

Activity of <c+a> dislocations has received much attention in many studies of the deformation of Y-containing Mg alloys [9, 10, 12, 13, 26, 27]. Due to the high CRSS of pyramidal <c+a> slip, it is usually activated in late deformation when <a> slip modes are strongly hardened and unable to accommodate local strain. In the present experiment, we mostly focus on the early deformation regime (strain<2%). The relatively weak texture of this Mg-5wt%Y alloy and the easiness for the cross-slip of <a> dislocations also mean that basal and non-basal <a> slip can probably accommodate plastic strain very well, which further reduces the necessity for <c+a>

slip to be activated. Nevertheless, we shall not exclude the possibility that <c+a> slip might have been activated in some grains with strong stress concentration. Those grains are unlikely though to develop continuous orientation rotation around a single axis, as the mobility of <c+a> dislocations are low and they often undergo non-planar dissociation [12, 29, 30] during their glide. TEM that can resolve dislocations in single grains would be a better technique to characterize <c+a> slip than the present 3DXRD technique.

To conclude, in an extruded Mg-5wt%Y alloy, we identified the activity of basal, prismatic and pyramidal <a> slip in different grains using in situ 3DXRD. The result was verified by ex situ EBSD-based slip trace analysis. The estimated ratio of $CRSS_{prism}/CRSS_{basal}$ is 1.8–2.7; the estimated ratio of $CRSS_{pyramidal\ <a>}/CRSS_{basal}$ is 1.6–1.8. Enhanced non-basal <a> slip can account for the high tensile ductility of the Mg-Y alloy.

This work is financially supported by the National Natural Science Foundation of China (No. 51631006 and No. 51671127). L.W. is also sponsored by Shanghai Pujiang Program. The Deutches Elektronen-Synchrotron (DESY) is acknowledged for providing the beamtime at the P07 beamline of PETRA III under proposal I-20150056.

REFERENCE

[1] H. Friedrich, S. Schumann, J. Mater. Proc. Tech. 117 (2001) 276.

[2] B.C. Suh, M.S. Shim, K.S. Shin, N.J. Kim, Scr. Mater. 84-85 (2014) 1.

[3] K. Hantzsche, J. Bohlen, J. Wendt, K.U. Kainer, S.B. Yi, D. Letzig, Scr. Mater. 63 (2010) 725.

[4] J. Bohlen, M.R. Nürnberg, J.W. Senn, D. Letzig, S.R. Agnew, Acta Mater. 55 (2007) 2101.

[5] Y. Chino, X. Huang, K. Suzuki, K. Sassa, M. Mabuchi, Mater. Sci. Eng. A 528 (2010) 566.

[6] N. Stanford, R. Cottam, B. Davis, J. Robson, Acta Mater. 78 (2014) 1.

[7] B. Raeisinia, S.R. Agnew, Scr. Mater. 63 (2010) 731.

[8] B. Raeisinia, S.R. Agnew, A. Akhtar, Metall. Mater. Trans. A 42A (2011) 1418.

[9] S. Sandlöbes, S. Zaefferer, I. Schestakow, S. Yi, R. Gonzalez-Martinez, Acta Mater. 59 (2011) 429.

[10] S. Sandlöbes, M. Friák, S. Zaefferer, A. Dick, S. Yi, D. Letzig, Z. Pei, L-F. Zhu, J. Neugebauer, D. Raabe, Acta Mater. 60 (2012) 3011.

[11] S.L. Shang, W.Y. Wang, B.C. Zhou, Y. Wang, K.A. Darling, L.J. Kecskes, S.N. Mathaudhu, Z.K. Liu, Acta Mater. 67 (2014) 168.

[12] S.R. Agnew, L. Capolungo, C.A. Calhoun, Acta Mater. 82 (2015) 255.

[13] K.-H. Kim, J.B. Jeon, N.J. Kim, B.-J. Lee, Scr. Mater. 108 (2015) 104.

[14] T.Tsuru, D.C. Chrzan, Sci. Rep. 5 (2015) 8793.

[15] H.F. Poulsen, J. Appl. Crystallogr. 45 (2012) 1084.

[16] J.C. Schuren, P.A. Shade, J.V. Bernier, S.F. Li, B. Blank, J. Lind, P. Kenesei, U. Lienert, R.M. Suter, T.J. Turner, D.M. Dimiduk, J. Almer, , Curr. Opin. Solid State Mater. Sci. 19 (2015) 235

[17] L. Wang, J. Lind, H. Phukan, P. Kenesei, J.-S. Park, R.M. Suter, A.J. Beaudoin, T.R. Bieler, Scr. Mater. 92 (2014) 35.

[18] T.R. Bieler, L. Wang, A.J. Beaudoin, P. Kenesei, U. Lienert, Metall. Mater. Trans. A 45 (2014) 109.

[19] H. Abdolvand, M. Majkut, J. Oddershede, J.P. Wright, M.R. Daymond, Acta Mater. 93 (2015) 246.

[20] H. Abdolvand, M. Majkut, J. Oddershede, S. Schmidt, U. Lienert, B.J. Diak, P.J. Withers, M.R. Daymond, Int. J. Plast. 70 (2015) 77.

[21] J. Oddershede, J.P. Wright, A. Beaudoin, G. Winther, Acta Mater. 85 (2015) 301.

[22] G. Winther, J.P. Wright, S. Schmidt, J. Oddershede, Int. J. Plast. 88 (2017) 108.

[23] H.O. Sørensen, S. Schmidt, J.P. Wright, G.B.M. Vaughan, S. Techert, E.F. Garman, J. Oddershede, J. Davaasambu, K.S. Paithankar, C. Gundlach, H.F. Poulsen, Z. Krist. 227 (2012) 63.

[24] S. Schmidt, J. Appl. Crystallogr. 47 (2014) 276.

[25] C.M. Cepeda-Jiménez, J.M. Molina-Aldareguia, M.T. Pérez-Prado, Acta Mater. 84 (2015) 443.

[26] J. Koike, Metall. Mater. Trans. A 36 (2005) 1689.

[27] D. Zhang, H. Wen, M.A. Kumar, F. Chen, L. Zhang, I.J. Beyerlein, J.M. Schoenung, S. Mahajan, E.J. Lavernia, Acta Mater. 120 (2016) 75.

[28] J.J. Bhattacharyya, F. Wang, P.D. Wu, W.R. Whittington, H. El Kadiri, S.R. Agnew, Int. J. Plast. 81 (2016) 123.

[29] Z.X. Wu, W.A. Curtin, Nature 526 (2015) 62.

[30] Z.X. Wu, B. Yin, W.A. Curtin, Acta Mater. 119 (2016) 203.

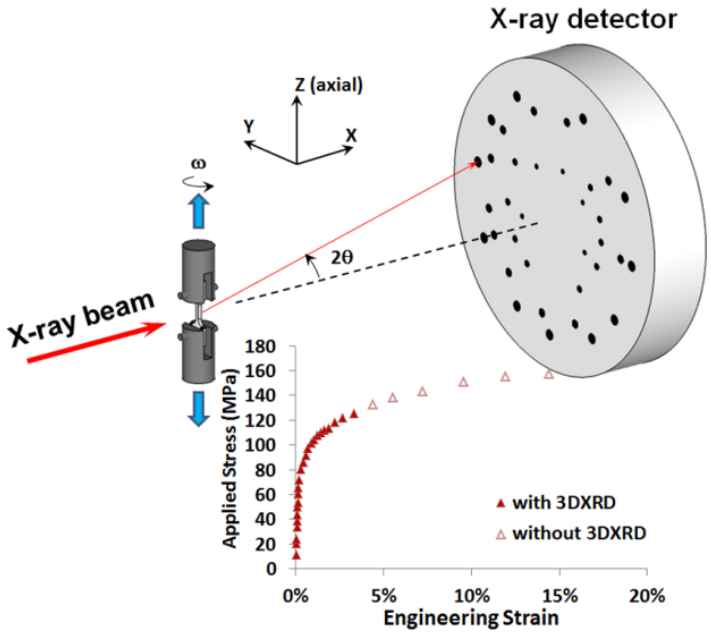

Figure 1. Schematic of 3DXRD experimental setup and the sample coordinate system for the data analysis. The tensile stress-strain curve of the specimen is also shown.

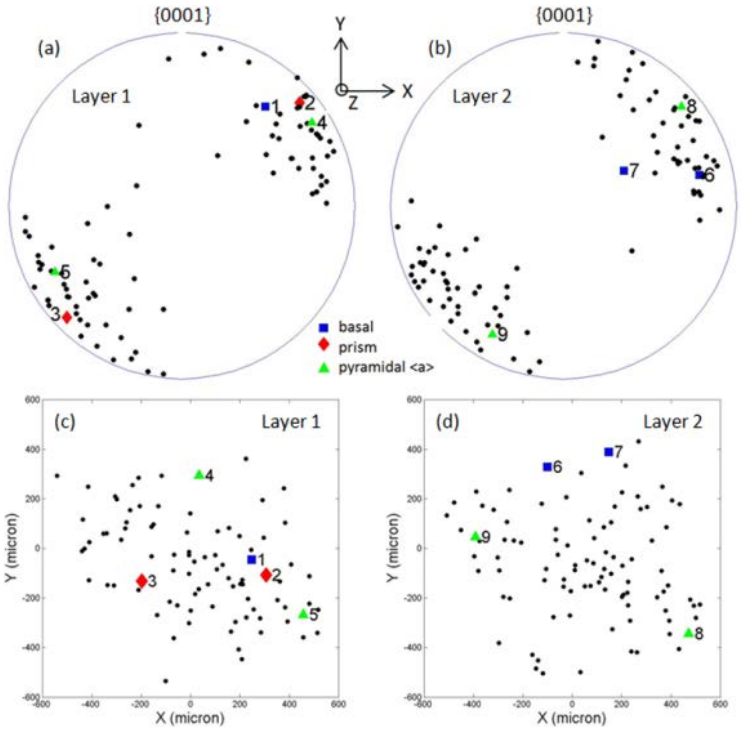

Figure 2. The {0001} pole figures and COM maps of the indexed grains in layer 1 (a, c) and layer 2 (b, d) at zero strain. The identified active slip modes in Grains 1–9 are marked.

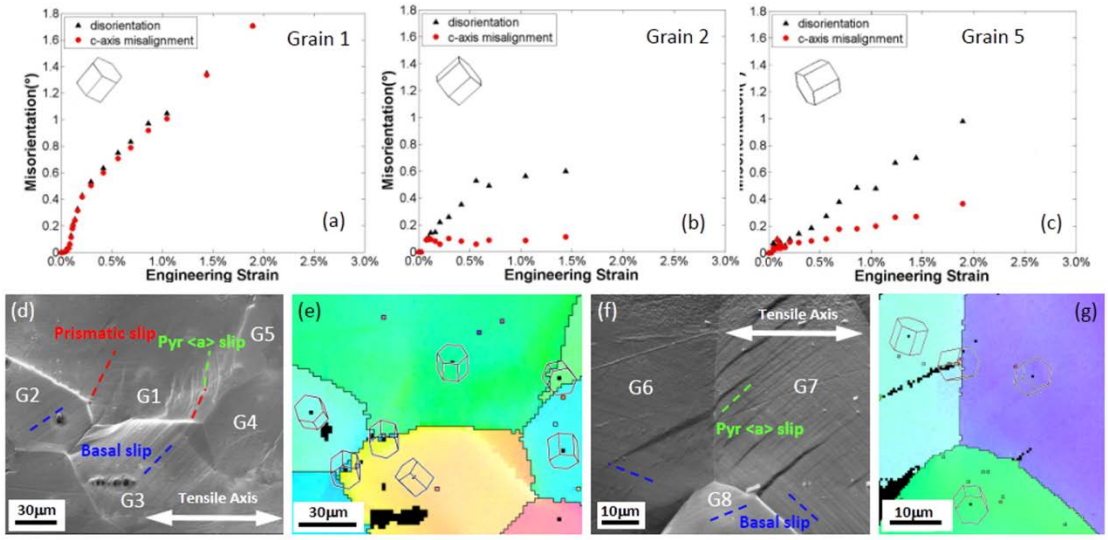

Figure 3. (a-c) Disorientation and c-axis misalignment evolution in Grains 1, 2 and 5 during deformation. A hexagonal prism at the top left of each figure represents the grain orientation. (d-g) EBSD based slip trace analysis of a separately deformed specimen shows slip lines from basal, prismatic and pyramidal <a> slip in different grains.

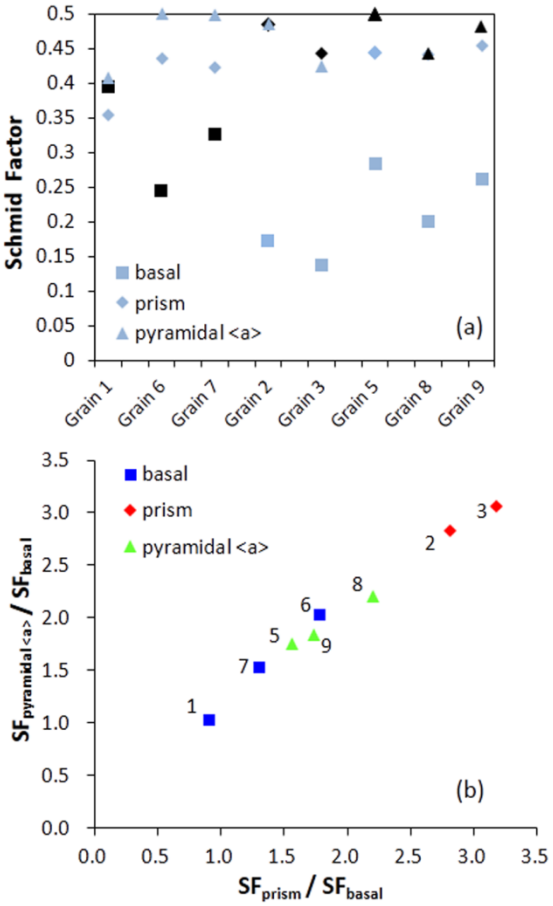

Figure 4. (a) SFs of basal, prismatic, and pyramidal <a> slip in Grains 1, 6, 7, 2, 3, 5, 8, and 9. For each grain, the actually activated slip mode is colored in black. (b) Ratios of $SF_{pyramidal\ <a>}$ / SF_{basal} and SF_{prism} / SF_{basal} in these grains.